Mapping DNA damage-dependent genetic interactions in yeast via orgy mating and barcode fusion genetics.

J. Javier Díaz-Mejía[1-4], Joseph C. Mellor[1-6], Atina Coté[1-3], Attila Balint[1,7,8], Brandon Ho[1,7], Pritpal Bansal[1-3], Fatemeh Shaeri[1-3], Marinella Gebbia[1,2], Jochen Weile[1-3], Marta Verby[1,3], Anna Karkhanina[1-3], YiFan Zhang[1-3], Cassandra Wong[3], Justin Rich[1-3], D'Arcy Prendergast[1-3], Gaurav Gupta[1-3], Sedide Öztürk[5,11], Daniel Durocher[2,3], Grant W. Brown[1,7], Frederick P. Roth[1-5,9,10]

[1] Donnelly Centre, University of Toronto, Toronto, ON M5S 3E1, Canada

[2] Department of Molecular Genetics, University of Toronto, Toronto, ON M5S 3E1, Canada

[3] Lunenfeld-Tanenbaum Research Institute, Mt. Sinai Hospital, Toronto, ON M5G 1X5, Canada

[4] Department of Computer Science, University of Toronto, Toronto, ON M5S 3E1, Canada

[5] Department of Biological Chemistry and Molecular Pharmacology, Harvard Medical School, Boston, MA 02115, USA

[6] Present address: seqWell, Inc. Beverly, MA 01915, USA

[7] Department of Biochemistry, University of Toronto, Toronto, ON M5S 3E1, Canada

[8] Present address: Center for Chromosome Stability, Department of Cellular and Molecular Medicine, University of Copenhagen, Copenhagen, Denmark

[9] Center for Cancer Systems Biology (CCSB) and Department of Cancer Biology, Dana-Farber Cancer Institute, Boston, MA 02215, USA

[10] Canadian Institute for Advanced Research, Toronto, ON M5G 1Z8, Canada

[11] Roche Sequencing Solutions, Pleasanton, CA 94588, USA

Abstract

Condition-dependent genetic interactions can reveal functional relationships between genes that are not evident under standard culture conditions. State-of-the-art yeast genetic interaction mapping, which relies on robotic manipulation of arrays of double mutant strains, does not scale readily to multi-condition studies. Here we describe Barcode Fusion Genetics to map Genetic Interactions (BFG-GI), by which double mutant strains generated via *en masse* orgy mating can also be monitored *en masse* for growth and genetic interactions. By using site-specific recombination to fuse two DNA barcodes, each representing a specific gene deletion, BFG-GI enables multiplexed quantitative tracking of double mutants via next-generation sequencing. We applied BFG-GI to a matrix of DNA repair genes under ten different conditions, including methyl methanesulfonate (MMS), 4-Nitroquinoline 1-oxide (4NQO), bleomycin, zeocin and four other DNA-damaging environments. BFG-GI recapitulated known genetic interactions and yielded new condition-dependent genetic interactions. We validated and further explored a subnetwork of condition-dependent genetic interactions involving *MAG1*, *SLX4,* and genes encoding the Shu complex, and found a new role for the Shu complex as a regulator of the checkpoint protein kinase Rad53.

Introduction

The importance of condition-dependent genetic interactions

Genetic interactions, defined by a surprising phenotype that is observed when mutations in two genes are combined [1], are powerful tools to infer gene and pathway functions [2,3]. Of the genetic interactions currently known in any species, the vast majority were found using Synthetic Genetic Array (SGA) technology in *Saccharomyces cerevisiae* [4–7] and these studies have yielded a rich landscape of genetic interactions. The sign of genetic interaction (defined to be negative when mutants are synergistically deleterious, and positive when the combination is less severe than would be expected from independent effects) provides clues about whether the genes act in parallel or in a concerted or serial fashion. Measuring similarity between genetic interaction profiles, both at the level of single genes and of clusters of genes, has revealed a hierarchical map of eukaryotic gene function [5,6]. However, the vast majority of genetic interaction mapping has been conducted under a single standard culture condition.

The importance and qualitative nature of gene function changes with environmental fluctuation, so that condition-dependent genetic interaction mapping is required. For example, pairs of DNA repair genes had different genetic interactions when cells were cultured in the DNA damaging agent methyl methanesulfonate (MMS) [4,8]. Further investigation revealed that there were 2-4 times more genetic interactions between DNA repair genes under MMS treatment compared with rich media alone. Different growth conditions are likely to reveal

different genetic interactions [3], suggesting that a plethora of condition-dependent genetic interactions remain to be uncovered by tripartite gene × gene × environment studies.

Current genetic interaction discovery technologies

Essentially every large-scale genetic interaction mapping strategy in yeast uses a genetic marker system developed for the SGA technique, which works by mating a single-gene deletion query strain with an array of different single-gene deletion strains from the Yeast Knockout Collection (YKO) [9]. The SGA system provided genetic markers by which mated diploids can be subjected to a series of selections to ultimately yield haploid double mutants. In 'standard' SGA mapping, the fitness of the resulting double mutants is determined computationally by imaging each plate to measure cell growth of each separately-arrayed strain[10]. SGA has also been used to study genetic interactions in functionally selected gene matrices [11] and applied to detect environment-dependent interactions [4]. St Onge *et al* [8] used the SGA markers to generate all pairwise double mutants between 26 DNA repair genes in yeast. In that study, the authors cultured each double mutant individually in microplates and monitored a time course of cell density to infer the fitness of the double mutants and identify genetic interactions in the presence and absence of MMS.

Others have measured genetic interactions via competition-based fitness measurements in liquid cultures, adding fluorescent markers for tracking cell viability, and using robotic manipulation to inoculate and measure cell growth

[12,13]. A recent technique called iSeq incorporated barcodes into single-mutant strains, such that pairs of barcodes identifying corresponding pairs of deleted genes could be fused by Cre-mediated recombination [14]. They demonstrated the method, showing that a pool corresponding to 9 gene pairs could be sequenced to monitor competitive growth of double-mutants *en masse* in different environments[14].

For each of the above methods, double mutants were generated by individual mating of two specific yeast strains, requiring at least one distinct location for each double-mutant strain on an agar or microwell plate and necessitating robotic strain manipulation to achieve large scale. By contrast, other methods to map genetic interaction generated double mutants in a one-vs-many fashion. For example, diploid-based synthetic lethality analysis on microarrays (dSLAM) [15] disrupted a single 'query' gene by homologous recombination via transformation of a marker into a pool of diploid heterozygous deletion strains bearing the SGA marker. After selecting for double-mutant haploids from such a 'one-by-many' haploid double-mutant pool, barcodes were PCR amplified from extracted double mutant DNA and hybridized to microarrays to infer the relative abundance and thus fitness of double mutants. Another method, Genetic Interaction Mapping (GIM) [16], generated a one-by-many pool of barcoded double mutants by *en masse* mating a single query strain to a pool of haploid gene deletion strains. Like dSLAM, GIM inferred strain abundance and fitness via barcode hybridization to microarrays. Despite the efficiency of generating one-by-many double-mutant pools, a matrix involving thousands of query strains would require thousands of such pools to be generated.

Each of the above methods has advantages and disadvantages. For example, measuring growth time-courses of each double-mutant strain provides high resolution fitness measurements [8,13], but scalability is low. Standard SGA is high-throughput, but requires specialized equipment for robotic manipulation, and these manipulations must be repeated to test genetic interaction in a new environment. The iSeq method shares the scaling challenge of SGA in strain construction, in that it requires many pairwise mating operations; however, once a double-mutant pool has been generated, it represents a promising strategy for measurement of competitive pools in different environments. The dSLAM and GIM methods allow generation of one-by-many pools, which reduces the number of mating operations, but both methods require customized microarrays as well as pool-generation and a microarray hybridization for every query mutation in the matrix.

Barcode Fusion Genetics to map Genetic Interactions (BFG-GI)

Here we describe BFG-GI, which borrows elements from several previous approaches. Like iSeq, BFG-GI requires generation of barcoded single-mutant strains, with only minimal use of robotics. To generate double-mutant pools, BFG-GI uses the SGA marker system. It is similar to the GIM strategy in that it employs *en masse* mating. Unlike GIM and all other previous genetic interaction mapping strategies, BFG-GI employs many-by-many 'orgy mating' to generate all double mutants for a matrix of genes in a single mating step. All successive steps are also conducted *en masse.* We show that double mutants can be generated and monitored in competitive pools using BFG-GI. Like iSeq, BFG-GI infers double mutant fitness in

competitively grown strain pools using next-generation sequencing of fused barcodes. Strain pools generated by orgy mating can be stored, and the aliquots can later be thawed and challenged under specific growth environments to detect condition-dependent genetic interactions without having to regenerate the double mutant strains. We assessed BFG-GI by mapping genetic interactions of DNA repair-related genes under multiple DNA-damaging conditions, revealing many condition-dependent interactions and a new function for the Shu complex in regulating the Rad53 checkpoint protein.

Results

BFG-GI experimental design overview

The first step in the BFG-GI process is generating uniquely barcoded donor and recipient strains from complementary mating types. Each donor and recipient contained *loxP/2272* sites to mediate barcode fusion using the Cre/Lox system after the mating step. We created donors by crossing individual gene deletion strains from the YKO collection with proDonor strains that contained newly constructed pDonor plasmids with unique barcodes flanked by *loxP/2272* sites (Fig 1A, S1 Fig and Materials and methods). We generated recipient strains by crossing individual gene deletion strains from the SGA query collection with proRecipient strains that contained unique barcodes flanked by *loxP/2272* sites (Fig 1B, S2 Fig and Materials and methods). Haploid selection of double mutants followed mating of donor and

recipient strains and *in vivo* fusion of barcodes using Cre/Lox recombination (Fig 1C).

We confirmed that barcode fusion occurred successfully using two neutral-insertion strains as controls (see Materials and methods for a definition of neutral loci). Specifically, we crossed a *MAT*alpha Donor *hoΔ::kanMX* to a *MAT***a** Recipient *ylr179cΔ::natMX* and induced Cre/Lox recombination to fuse their barcodes. After sporulation and selection of the *MAT*alpha haploid double mutant progeny (Materials and methods), we extracted genomic DNA, amplified barcode fusions by PCR and confirmed their integrity by Sanger sequencing (Fig 1C).

To scale up the BFG-GI process, we generated double mutants with unique fused barcodes *en masse* (detailed below). We selected hundreds of double mutants using a series of marker selection steps in a many-by-many fashion. Intermediate selection steps allowed us to fuse barcodes representing each donor and recipient parental pair within each double mutant cell (Fig 1D and Materials and methods).

Once we generated the pool of fused-barcode double mutants, aliquots were stored at -80°C for future experiments. Amplification and next-generation sequencing of fused barcodes in the pool allowed us to infer the relative abundance of each double mutant in each condition of interest (Fig 1D and Materials and methods). In addition to haploid double mutant pools, we sequenced fused barcodes from the heterozygous diploid double mutant pools and used those as reference ('time zero') controls for fitness and genetic interaction calculations (Materials and methods).

BFG-GI measures the strain abundance profile of a heterogeneous cell population

We first evaluated the ability of BFG-GI to accurately detect the abundance of double mutants. To generate reference data for this evaluation, we used the array-based SGA strategy to generate 2,800 double mutants by individual mating of barcoded BFG-GI strains, subsequently inducing barcode fusion via the Cre/Lox system. We recorded colony sizes, scraped plates to pool all double mutant cells, extracted genomic DNA, and sequenced the fused barcodes (Materials and methods). The resulting numbers of sequencing reads for each strain was strongly correlated with the corresponding colony sizes (R=0.92, Fig 2A). Importantly, very small or absent colonies correlated with double mutants with very few or no sequencing reads. These results show that BFG-GI detects the abundance of specific double mutants in pools of cells, with results comparable to an array-based method.

Generating a DNA repair-focused double-mutant strain pool

To test whether BFG-GI can accurately map genetic interactions, we generated a double mutant pool focused on DNA repair genes and compared BFG-GI results to those of other validated genetic interaction assays. We began by generating donor and recipient strains by crossing 35 YKO (*yfg1Δ::kanMX, MAT***a**) single gene deletion strains to BFG-GI proDonor strains, and 38 SGA query (*yfg2Δ::natMX, MAT*alpha) single gene deletion strains to BFG-GI proRecipient strains (Fig 1). These strains included 26 DNA repair genes from a previous condition-dependent genetic

interaction study [8], as well as 14 likely-neutral loci (e.g. the already-disrupted *HO* locus, pseudogenes, and other loci for which single- and double-mutant phenotypes have not been previously observed). Inclusion of neutral loci allowed us to infer single mutant fitness from pools of double mutants (Materials and methods).

To generate haploid double mutants, donor and recipient cells were scraped from plates and all subsequent steps in the BFG-GI pipeline were conducted *en masse*. First, the pools were combined for 'orgy mating'. Seven selection steps followed mating, including four that correspond to those in the standard SGA procedure: heterozygous diploid selection, sporulation, *MAT***a** progeny selection, and haploid double mutant selection. Additionally, before sporulation, we completed three selection steps to fuse barcodes and subsequently remove Cre to limit undesired recombination events (Fig 1C and S3 Fig). This generated a pool of 4,288 haploid double mutants, which was aliquoted and stored as frozen glycerol stock. Thawed samples were used to inoculate solid media appropriate for selecting haploid double mutant cells. The media was used alone, supplemented with dimethyl sulfoxide (DMSO) as a control, or supplemented with one of eight drugs targeting DNA repair pathways (S1 Table). We extracted genomic DNA, amplified and sequenced fused barcodes to infer the relative abundance of each double mutant in each condition.

To evaluate assay reproducibility, we ran all BFG-GI procedures in duplicate, starting from the mating step (technical replicates) and also barcoded multiple strains representing the same gene (biological replicates). Biological replicate strains had either the same or different parental strain origin (the parental strain

for a given gene deletion might be from either the YKO or SGA query strain collection). Relative strain abundance was highly correlated between technical replicates (R > 0.95) and thus we decided to combine technical replicates for subsequent analyses. Next, we used a multiplicative model [1] to infer a genetic interaction score (GIS) from relative strain abundances (Materials and methods).

Correlation of GIS profiles between biological replicates representing the same gene were in general high, with 85% of replicates showing GIS R>0.5. We computationally excluded 20 biological replicates showing correlations below this cutoff from analysis and the remaining same-gene biological replicates showed correlations that were clearly distinct from strain pairs representing different genes (Fig 2B). Most replicates showing GIS R<0.5 were recipients. To understand factors contributing to uncorrelated pairs we sequenced the genomes of 10 strain pairs with GIS R<0.5 and another 10 with GIS R>0.5. We found that all 10 strains with GIS R<0.5 had chromosome V duplicated, in agreement with the report of iSeq strains that show low reproducibility [14]. Chromosome V contains the *CAN1* locus, which is where both BFI-GI recipients and iSeq strain constructs were inserted. In contrast, only 3 out of 10 strains with R>0.5 showed aneuploidies (also in chromosome V). All BFG-GI strains showing aneuploidies were recipients. This suggests that future versions of BFG-GI recipients for which selection markers are carried by plasmids may increase reproducibility, as we found for our Donor strains.

Our final dataset consisted of 3,360 double mutants, with 60 Donors and 56 Recipients, representing 39 genes (25 DNA repair genes and 14 neutral genes; S2

Table). Replicates representing *SWC5* showed very low relative abundance in the sequencing results and were removed from subsequent analyses.

We evaluated the performance of BFG-GI measurements by contrasting our GIS for no-drug and MMS conditions (two conditions commonly used as gold standards in genetic interaction studies) against Epsilon scores for these same conditions [8]. We found that GIS and Epsilon scores correlated well with each other in both conditions: no drug R=0.57 and MMS R=0.75 (Fig 2C and Fig 2D). Furthermore, at a false positive rate of 20%, BFG-GI showed a sensitivity of 50% for detecting positive genetic interactions and 70% for detecting negative genetic interactions (Fig 2E).

Finally, we assessed the ability of BFG-GI to predict the relative abundance of three classes of double mutant strains. First, we measured the abundance of double mutant strains with mutations in the same gene. Heterozygous diploid double mutants for the same gene (e.g. *MMS4/mms4Δ::kanMX mms4Δ::natMX/MMS4*) can survive in media supplemented with selective antibiotics, but haploids should not survive because they have only one locus for each gene and thus are not expected to carry both antibiotic resistance markers. Thus, haploid strains for same-gene pairs are expected to behave like synthetic lethal combinations and be depleted from the pools. Our BFG-GI sequencing results agreed with this hypothesis (Fig 2F). Second, we assessed the abundance of double mutants representing pairs of linked genes (<30 kbp apart). Independent segregation is reduced between linked genes, and as expected our BFG-GI quantitation measurement by sequencing indicated these double mutants were depleted from the pools (Fig 2F). Last, we analyzed double

mutants representing unlinked genes and we found that their GIS distribution is clearly distinguishable from same-gene and linked gene pairs (Fig 2F).

Taken together, these results provide evidence that BFG-GI is a powerful tool to generate double mutants by mating *en masse* and to monitor strain abundance to infer condition-dependent genetic interactions.

BFG-GI reveals condition-dependent genetic interactions

Having determined that BFG-GI can accurately detect genetic interactions, we analyzed the DNA-repair focused double mutant pool under 10 culture conditions (S1 Table) to identify condition-dependent genetic interactions. We applied an absolute Z-score of GIS=1 as a cutoff to identify positive and negative genetic interactions in each of the 10 conditions (S1 Table and S2 Table). We found that although almost all genes showed at least one genetic interaction, some genes showed markedly more interactions than others. For example, we found that the DNA helicase gene *SGS1* paired with *MMS4, MUS81* or *SLX4* (all of which participate in template switching during break-induced replication) yielded negative interactions in all 10 conditions (Fig 3A). Another DNA helicase gene, *SRS2*, interacted negatively with both *SGS1* and the DNA translocase gene *RAD54* in all 10 conditions. By contrast, both *SGS1* and *SRS2* showed positive genetic interactions in most conditions with *RAD5* and *RAD57*, which are involved in error-free DNA damage tolerance and recombinational repair of double-strand breaks, respectively. These findings coincide with previous reports showing *SGS1* and *SRS2* centrality in DNA repair pathways in both unperturbed and MMS-induced stress conditions [8].

We identified condition-dependent genetic interactions by comparing GISs between each pair of conditions. For example, we found *mus81Δ/rad5Δ* displayed a negative GIS in DMSO and a positive GIS in MMS. This change is shown as a red edge in Fig 3B, panel *i*, and agrees with a previous report [8]. By contrast, most changes in genetic interactions between DMSO and MMS were from neutrality in one condition to either positive or negative GIS in the other (Fig 3B, panels *i* and *iv*). In fact, when we extended this analysis to include all pairwise condition comparisons we found that that the vast majority of genetic interaction changes (>95%) were from neutrality in one condition to either positive or negative GIS in the other condition; less than 5% of genetic interactions changed from positive in one condition to negative in the other (Fig 3C).

As expected, the two conditions most similar to each other were no-drug and DMSO, which showed only eleven sign changes, all from neutrality to either positive or negative GIS (S1 Table). Among the eight drugs, cisplatin showed the least changes compared with DMSO or no drug conditions (53 and 50 sign changes, respectively), followed by bleomycin and zeocin (each exhibiting 52 sign changes), which are members of the same family of glycopeptides that intercalate into DNA to induce double strand breaks [17]. In contrast, condition pairs showing the highest number of sign changes include camptothecin vs. either 4NQO or MMS (each with 84 sign changes). These data are consistent with the fact that these drug pairs have different mechanisms of action and cause DNA lesions that are repaired by different pathways.

A condition-dependent subnetwork with *MAG1*, *SLX4* and Shu complex genes

The Shu complex (a heterotetramer consisting of Csm2, Psy3, Shu1, and Shu2) promotes Rad51 filament formation and homologous recombination during error-free lesion bypass, double strand break repair, and meiosis [18–22] (Fig 4A). Our BFG-GI results indicated that genes encoding all four members of the Shu complex showed negative genetic interactions with both *MAG1* and *SLX4* during exposure to MMS. Additionally, the Shu complex genes interacted negatively with *SLX4* during treatment with 4NQO, bleomycin and zeocin (Fig 4B). Mag1 is a 3-methyladenine DNA glycosylase that removes alkylated bases from DNA to initiate base-excision repair (BER), thereby protecting cells against alkylating agents like MMS [23,24]. Slx4 promotes the activity of three structure-specific endonucleases [25–28] and, upon exposure to MMS, plays a key role in down-regulating phosphorylation of the checkpoint kinase Rad53 [29,30]. We generated double mutants for each Shu complex member with either *MAG1* or *SLX4* and tested their fitness on media containing DMSO or various genotoxins using spot dilution assays (Fig 4C). Our results validated the *MAG1*-Shu complex interaction in MMS that we detected with BFG-GI, and are consistent with a previous study [31]. The negative interactions between *MAG1* and Shu complex members are explained by the simultaneous loss of Mag1-mediated BER that directly removes alkylated bases and decreases in error-free lesion bypass, a major pathway used during MMS-induced DNA replication blocks [32], in the double mutants [31] (Fig 4A). Our spot dilution assays also confirmed that *MAG1* interacts negatively with *SLX4* during MMS

treatment, in agreement with a previous study showing that BER is unlikely to be the major function of *SLX4* [25]. Of particular interest, we validated the BFG-GI interactions between Shu complex members and *SLX4* during treatment with MMS, 4NQO, bleomycin, or zeocin (Fig 4C). As the nature of the *SLX4* interactions with Shu complex genes is unknown, we decided to study them in more detail.

The negative genetic interactions between *SLX4* and Shu complex members in MMS were unexpected, given that the Shu complex promotes error free lesion bypass [18,21,31,33] and *SLX4* shows epistatic relationships with error-free lesion bypass genes during MMS treatment [25]. A major role for Slx4 during MMS treatment is in the down-regulation of Rad53 phosphorylation and activation, which occurs by Slx4 competing with Rad9 for binding to Dpb11 in order to limit the formation of Rad9-Dpb11 complexes that activate Rad53 [29,30,34,35]. Cells deleted for *SLX4* or *PPH3*, which encodes the catalytic subunit of the protein phosphatase PP4 complex that binds and dephosphorylates Rad53 during MMS treatment [36], display hyperactivation of Rad53 upon MMS treatment and sensitivity to MMS that is suppressed by expression of a hypomorphic *rad53-R605A* allele defective for full Rad53 activation [29,30,34]. In *slx4Δ pph3Δ* cells, Rad53 hyperactivation is further elevated and these double mutants display synergistic sensitivity to MMS [29]. To determine whether the genetic interactions between *SLX4* and Shu complex members reveal an unanticipated role for the Shu complex in regulating Rad53-P levels (Fig 4D), we tested the sensitivity of *pph3Δ*/Shu complex double mutants to MMS using spot dilution assays. Combining *pph3Δ* with deletion

of any of the Shu complex genes resulted in a dramatic increase in MMS sensitivity relative to the single mutants (Figs 4C and 4E), indicating negative genetic interactions similar to those seen between *SLX4* and Shu complex members (Fig 4C), or between *SLX4* and *PPH3* [29].

To assess MMS-induced Rad53 activation in Shu complex mutants more directly, we monitored Rad53 phosphorylation (which is a proxy for Rad53 activation) using western blot assays. Consistent with the role of *SLX4* in dampening Rad53 activation [29,30,37], *slx4Δ* cells challenged with MMS showed an increase in Rad53-P levels relative to wild type (Fig 4F). Interestingly, three of the Shu complex mutants (*csm2Δ*, *psy3Δ*, and *shu1Δ*) also showed an increase in Rad53-P levels upon treatment with MMS (Fig 4F), indicating that these Shu complex mutants, like *slx4Δ* and *pph3Δ* cells, display hyperactivated Rad53 under exposure to MMS. We asked whether the MMS sensitivity of Shu complex mutants could be suppressed by expression of the *rad53-R605A* allele. Expression of *rad53-R605A*, which is not effectively hyper-activated, suppresses the MMS sensitivity of *slx4Δ* and *pph3Δ* [29,30]. Similarly, the MMS sensitivity of *csm2Δ, psy3Δ, shu1Δ* and *shu2Δ* mutants was partially suppressed by *rad53-R605A* (Fig 4G). Together, our data indicate that the Shu complex, like Slx4 and Pph3, regulates Rad53 activation in response to MMS treatment, as revealed by unique condition-dependent genetic interactions detected by BFG-GI.

Discussion

We developed a new technology, called BFG-GI, in which pools of double mutant yeast strains corresponding to a matrix of target genes are generated *en masse* through many × many 'orgy mating'. These pools are induced to form double-mutant-identifying chimeric barcodes by intra-cellular site-specific recombination, and assayed for growth via next-generation sequencing. Aliquots of these pools can be stored, and later cultured with different drugs to identify condition-dependent genetic interactions. To our knowledge, BFG-GI is the first method to generate haploid double-mutant strains *en masse* for a many × many matrix of genes without the requirement for multiple mating steps, thus enabling large-scale conditional genetic interaction mapping without extensive use of robotics.

BFG-GI showed good agreement with previous methods in mapping genetic interactions commonly used to benchmark genetic interaction technologies. Correlation (R) with existing data was 57-75%, with 50-70% of previous interactions being captured at an apparent false positive rate (1-specificity) of 20%. This false positive rate is conservative, in that potentially novel true interactions are treated as false positives. We detected and validated unanticipated interactions between the Shu complex and *SLX4,* and found that the Shu complex dampens Rad53 activation during MMS treatment. Thus, our results provide evidence for a previously uncharacterized role of the Shu complex in the cellular response to DNA damage by MMS.

We calculated similarity between the genetic interaction matrices of different drugs, and found that those with similar mechanisms of action, like zeocin and bleomycin, are considerably more similar to each other than those with different mechanisms of action, like MMS and camptothecin. This suggests the potential of BFG-GI to shed light on drug mechanisms through measurement of gene-gene-environment interactions.

One advantage of BFG-GI is its cost-effectiveness. BFG-GI uses fewer reagents and less robotic assistance than other technologies to map genetic interactions because it is a pool-based technology. Pool-based technologies require less media, plates, and drugs than array-based technologies, a substantial cost advantage particularly when the price of drugs is factored in. For example, the amount of media used in 1536 spot arrays on OmniTrays is reduced 50-fold by studying the same number of gene-pairs in 100 OD pooled cultures in 143 cm^2 Petri dishes (optimal cell density for pooled double mutant selections). BFG-GI is also more cost-effective than other barcode-sequencing technologies because in BFG-GI, strains are pooled at the mating step, rather than generating strains using robotically manipulated strain arrays.

The reproducibility of BFG-GI indicates that it is a robust technology. Technical replicates in BFG-GI are highly reproducible, and 85% of the biological replicates correlated well with each other (GIS R>0.5). The remaining 15% of biological replicates showing low correlations could be identified and removed computationally. We concur with the iSeq study [14] that aneuploidies in chromosome V are the main factor contributing to the replicates with low

reproducibility. Chromosome V carries both *CAN1* and *URA3* loci, which were replaced by selection markers in the iSeq protocol [14], while *CAN1* was replaced by the recipient constructs in BFG-GI. Thus, *de novo* mutations around these loci during strain construction could explain the low correlation between some pairs of biological replicates. This possibility is supported by our observation that almost all BFG-GI strains showing GIS R<0.5 were recipients, whereas donors –for which constructs are carried on plasmids– showed GIS R>0.5. In the BFG-GI protocol, once the donor and recipient barcodes are fused, the relic donor plasmid is counter-selected with 5-FOA to reduce the chance of undesired recombination events. We concur with Jaffe *et al.* [14] who suggest that future protocols using constructs located on plasmids, such as the one we used with the proDonor strains, or in other chromosomal loci may serve to eliminate this issue. Notwithstanding this issue, however, the BFG-GI method proved to be highly accurate in comparisons with previous benchmark studies.

We took several steps to reduce the chance of undesired strains in BFG-GI from taking over pooled cultures, including optimization of both mating and sporulation, and adapting protocols and constructs reportedly improving the selection of the *MAT***a** double mutant progeny in SGA. For example, mating and sporulation are the two primary population bottlenecks when generating haploid double mutants by meiotic segregations, and they must be optimized to maintain a pool complexity that is large enough to interrogate all desired gene-gene combinations. Optimizing these two processes is also important to reduce potential jackpot effects in the pool cultures (i.e. to avoid strains with genetic anomalies to

take over the entire pool growth). We elaborated on previous studies to optimize mating [38] and sporulation [39] for our culture pools. We found that cell density was a key factor for mating efficiency (3% using 300 ODs vs. 22% using 30 ODs, in the same mating area, Materials and methods). Similarly, the time allowed for sporulation dramatically affected its efficiency (4% at 5 days vs. 18% at 12 days). Furthermore, we used the *STE2* and *STE3* promoters currently used for SGA to select for haploid cells which have been reported to perform better than earlier alternatives (e.g. *MFA/MFalpha* promoters*)* [40]. We used these constructs to first select the *MAT***a** progeny from sporulation cultures and then the haploid double mutants. Using *STE2/STE3* promoters, optimizing mating and sporulation, and using an intermediate *MAT***a** selection step between sporulation and haploid double mutant selection together likely reduced the number of mitotic crossover survivors and jackpot mutation effects in our pools.

BFG-GI is a flexible technique that can be used in the future to identify genetic interactions in many different settings. Generation of BFG-GI proDonor and proRecipient strains is one of the most time consuming steps in our pipeline because it includes sequence verification of both *loxP/lox2272* sites and barcodes. However, once generated these proDonor and proRecipient "toolkits" can be used many times to create donor and recipient strains representing different genes with minimal robotic manipulation. We anticipate that BFG-GI will be a valuable technology to map condition-dependent genetic interactions in yeast and, as next-generation sequencing costs continue to decrease, BFG-GI can be expanded to

interrogate pools of double mutants representing bigger sets of gene pairs, including full genome combinations, across multiple conditions.

Materials and methods

Selected DNA repair and neutral gene strains

We retrieved strains representing 26 DNA repair genes whose null mutants were sensitive to MMS [8] from the YKO and SGA query collections. Additionally, 14 other loci deemed neutral because their null mutations did not affect cell fitness, were selected (S4 Fig). These 14 loci have few or no genetic interactions in genome-scale screens [5] and we did not find growth defects upon deletion of any of them.

BFG-GI toolkit strains

Donor toolkit construction

We constructed donor strains by generating two DNA fragments with overlapping ends which were co-transformed into yeast where they recombined generating pDonor constructs (S1 Fig). The first fragment, called preD1, contained the hygromycin resistance gene (*HygR)* driven by the *Schizosaccharomyces pombe TDH1* promoter and terminator, a unique barcode, *loxP/2272* loci, and flanking primer sites. First, we used a Gibson assembly [41] to produce plasmid pFR0032 with the P_{spTDH1}-*HygR*-T_{spTDH1} backbone. Then, we used three consecutive PCRs to add barcodes, priming sites, *loxP/2272* loci, and in-yeast recombination adapters (S1A Fig). The second fragment, preD2, contained the *URA3* marker and Cre recombinase driven by $P_{tetO\text{-}CMV}$. We generated this fragment by Gibson assembly of pFR0026, followed by a PCR to add in-yeast recombination adapters (S1B Fig). Then preD1

and preD2 fragments were co-transformed into yeast strain RY0771 (derived from BY4742) and merged by in-yeast assembly to generate pDonor plasmids (S1C Fig). We arrayed transformant strains to extract DNA and sequenced the preD1 loci, and proceeded with those strains containing confirmed preD1 loci. We mated selected *MAT*alpha proDonors with *MAT***a** deletion strains of interest (*i.e.* DNA repair or neutral genes) from the YKO collection (S1D Fig). A series of selective passages (S1D Fig and S3 Fig) resulted in Donor strains with the relevant genotype: *MAT*alpha *lyp1Δ::*P_{STE3}*-LEU2 his3Δ1 leu2Δ0 met17Δ0 ura3Δ0 yfg1Δ::kanMX pDonor(*$P_{tetO\text{-}CMV}$*-Cre lox2272* P_{TDH1}*-HygR-*T_{TDH1} *barcode loxP* P_{URA3}*-URA3 CEN/ARS* P_{AmpR}*-AmpR ori).*

Recipient toolkit construction

We constructed recipient strains using a method based on the *delitto perfetto* construct [42] to enhance homologous recombination of contructs as follows. First, we used consecutive PCRs to produce a fragment preR1, containing the *Kluyveromyces lactis URA3* gene, flanked by *loxP/2272* sites, unique barcodes and a sequence complementary to the *S. cerevisiae CAN1* locus (S2A Fig). Second, we incorporated the P_{STE2}*-spHis5-*T_{STE2} into the *CAN1* locus of the strain BY4741. Then the *delitto perfetto* construct was inserted upstream of the *MAT***a** selection reporter of the same strain (S2B Fig) to enhance homologous recombination of preR1 fragments. This generated a pool of RY0766 proRecipient strains (S2C Fig). We isolated and arrayed monoclonal proRecipient strains then sequenced and selected strains with intact preR1 loci. Selected *MAT***a** proRecipients were mated with

*MAT*alpha strains of the SGA query collection representing DNA repair and neutral genes (S1D Fig). A series of selective passages (S2D Fig and S3 Fig) resulted in recipient strains with the relevant genotype:

*MAT***a** *his3Δ1 leu2Δ0 met17Δ0 lyp1Δ ura3Δ0 can1Δ::barcode loxP klURA3 lox2272* P_{STE2}*-spHis5-*T_{STE2} P_{CMV}*-rtTA I-SceI* P_{GAL1}*-ISceI yfg2::natMX*

Generation of BFG-GI double mutants

Mating optimization for en masse *BFG-GI*

We focused on optimization of cell density for *en masse* orgy mating because previous evidence shows cell density influences mating efficiency [38]. We determined the optimal cell density for *en masse* orgy mating by inoculating mating Petri dishes with a mixture of two neutral strains (*MAT*alpha Donor *hoΔ:: kanMX,* and *MAT***a** Recipient *ylr179cΔ::natMX)* at cell densities varying from 30 OD to 300 OD and counting the colony forming units (CFUs). After generating mating mixtures, we took samples at 0 and 12 hours (hrs) of incubation at 23°C, and inoculated plates with either non-selective or heterozygous diploid double mutant selective media and counted CFUs. The ratio of CFUs in non-selective vs. selective media indicated that inoculating a 58cm^2 Petri dish with 30 ODs of mating mixture results in 22% mating efficiency. In contrast, 100 ODs of mating mixture results in 13% mating efficiency, and 300 ODs of mating mixture results in 3% mating efficiency. Hence, we used 0.51 ODs of mating mixture per cm^2 of plate for further *en masse* orgy matings.

To generate pools of double mutants, we arrayed BFG-GI donors and recipients in their respective selective media and cultured at 30°C for 48 hrs (S3 Fig). We made one pool for each mating type by scraping cells from plates into cultures; we normalized cell densities with sorbitol 1M to have equal number of cells per strain (50 ODs per mL) and we lightly sonicated cells to disrupt clumps (Branson microtip sonicator, 10% duty cycle, output 2, 25 bursts, pause of 3 sec., and a second 25 bursts). We mixed the two pools together by stirring them in a flask for 10 min. Finally, we inoculated two Bioassay dishes (500cm^2) with 259 ODs each of the mating mixture, and mating cultures were incubated for 12 hrs at 23°C.

Generation of heterozygous diploid double mutants, induction of barcode fusion and pDonor elimination

The generation of the heterozygous diploid double mutants required passaging the mating progeny every 24 hrs in selective media. Passages included selection of heterozygous diploid double mutants, induction of the Cre/Lox system with doxycycline, counter-selection of the relic pDonor with 5-FOA, and recovery from 5-FOA counter-selection to increase sporulation efficiency (S3 Fig).

*Generation of MAT***a** *haploid double mutants with fused barcodes*

We used cultures recovered from 5-FOA counter selection to inoculate liquid PRE5 pre-sporulation media for 2 hrs at 30°C to induce exponential growth, then spun down the cells and transferred them to SPO2 sporulation media [39] supplemented with histidine, leucine, methionine and uracil to mask BFG-GI strain auxotrophies at

concentrations used in the SGA sporulation protocol [10]. We incubated sporulation cultures at 21°C for 12 days. This resulted in ~18% sporulation efficiency, as evaluated by counting CFU's in non-selective and selective media and tetrad visualization. Shorter incubation periods reduced the sporulation efficiency (~4% at 5 days, ~13% at 7 days). Finally, we selected the *MAT***a** haploid progeny from sporulation cultures, followed by haploid double mutant selection. Aliquots were stored in glycerol at -80 degrees for future use.

Exposure of pooled cultures to drugs

Before challenging haploid double mutant pools to drugs we identified the appropriate drug concentration for our experiment by exposing a neutral BFG-GI haploid double mutant (*hoΔ::kanMX/ ylr179cΔ::natMX*) in growth assay liquid cultures to various drug concentrations. We selected drug doses corresponding to 20% of the minimal inhibitory concentration for the neutral test strain (S1 Table). To expose mutant strains to drugs we thawed frozen haploid double mutant pools, allowed the pools to recover for 2 hrs in haploid double mutant liquid media at 30°C, and then used 100 ODs of this culture to inoculate 143cm^2 petri dishes containing solid media supplemented with each DNA repair drug. We cultured pools at 30°C for 24 hrs and then collected samples to sequence fused barcodes and thus infer each double mutant abundance.

Generation of BFG-GI double mutants in an array format

Mating and selecting donor and recipient strains for an array format was similar to the pool-based *en masse* orgy assay described above, but in this case we used robotic assistance to pairwise mate each donor with an array of recipients. We completed all steps, including sporulation, on solid media, and imaged the final haploid double mutant selection plates. We scraped cells from the final selection plates to sequence the fused-barcode population which allowed us to compare colony sizes with numbers of sequencing reads.

Next-generation sequencing and mapping of fused barcode pairs

The BFG-GI technology relies on the Cre/Lox system to recombine the complementary donor and recipient *loxP/lox2272* sites that flank the barcodes (Fig 1). We sequenced the fused barcodes from pools of cells using the following steps: 1) genomic DNA extraction using glass beads and phenol/chloroform, 2) PCR amplification of the 325 bp barcode fusion product with multiplexing sequencing adapters, 3) concentration and gel purification of the amplicon using 2% E-Gel EX agarose 2% (Invitrogen), DNA Clean & Concentrator Kit (Zymo Research) and MinElute Gel Extraction Kit 50 (Qiagen), 4) quantification of the DNA library by qPCR, and 5) sequencing by Illumina NextSeq paired-end technology. We mapped sequencing *.fastq files against the library of expected barcode sequences using the program Segemehl (v0.1.7, -A 85) and custom scripts; 97% of all sequencing reads mapped to expected barcodes.

Whole-genome sequencing and detection of chromosome duplications

Genomic DNA from 20 strains (S2 Table) was extracted by cell wall disruption with Zymolyase 100T 10mg/ml (Amsbio) and purified using AMPure beads (Agilent). gDNA was quantified with Quant-it Picogreen dsDNA assay kit (Invitrogen) and normalized to 2ng/ul for DNA fragmentation and library normalization with a Nextera XT DNA Library Prep Kit, using a transposase (Tn5) for tagmentation. A limited-cycle PCR was used to add Illumina sequencing adapters and indices i5 and i7. PCR amplicons with size between 400 and 800 bp were gel purified using a 2% E-Gel EX agarose 2% (Invitrogen) and MiniElute Gel Extraction kit (Qiagen). Whole genome sequencing was conducted on an Illumina NextSeq 500 using a HighOutput 150 cycles v2 kit with 40x coverage. Sequencing results were mapped against the reference genome UCSC sacCer3 (SGD vR64.1.1), corrected for GC content, and chromosomal duplications detected with the HMMcopy R package [43].

Retesting double mutant construction and spot dilution assays

We generated double mutant strains for retesting in spot dilution assays by mating single mutant *MAT*alpha SGA queries with *MAT***a** YKO collection strains, the exceptions being the *MAT***a** *RAD53* (MBS1437) and *rad53-R605A* (MBS1440) strains with the *RAD53* loci linked C-terminally to a *6xHis-3xFLAG-kanMX6* tag and resistance marker [30]. Next, we induced sporulation of heterozygous diploid double mutants as we did for BFG-GI strains. To confirm segregation of *kanMX* and *natMX* markers we manually dissected haploid double mutants from tetrads and verified segregation using both selective media and PCR. Sanger sequencing

confirmed residue 605 of *RAD53* and *rad53-R605A* strains. We grew strains overnight to saturation in liquid media, diluted them 1:10, and then used 1:5 serial dilutions for the spot assays. All cultures used YPD media supplemented with indicated drug concentrations.

Definition of Genetic Interaction Score (GIS)

Calculating relative abundance of strains from fused-barcode sequencing counts

We counted the total number of reads (C) for the donor (i) and recipient (j) barcode pairs (ij) in each condition-specific pool (k), and then divided by the total number of barcode counts in each k :

$$F_{ijk} = C_{ijk} / \sum_{ij} C_{ijk}$$

We also calculated the marginal frequencies (M) for each barcode:

$$M_{ik} = \sum_j F_{ijk} \quad \text{and} \quad M_{jk} = \sum_i F_{ijk}$$

Inference of single mutant abundance

First we contrasted the relative abundance of each barcode with measurements from the heterozygous diploid pool (h), which we used as a 'time zero' reference control.

$$R_{ik} = \frac{M_{ik} + \beta}{M_{ih} + \beta} \quad \text{and} \quad R_{jk} = \frac{M_{jk} + \beta}{M_{jh} + \beta}$$

β is a pseudocount-based regularization parameter such that: $\beta = \frac{\alpha}{\sum_{ij} C_{ijk}}$ and α is the number of pseudocounts used to avoid overestimating poorly measured barcode

pairs. Values for α between 1 and 10 were tested and no major differences were found in terms of benchmarking against previously published datasets [8] (described below), therefore α=1 was used.

Strains grown in selective pools of haploid double mutants need the two gene deletion markers *kanMX* and *natMX* to survive, therefore, we approached the single mutant and wild type relative abundance by using measurements for neutral genes (S4 Fig) in *k* and *h* pools. For the wild type inference we used:

$$R_{wt,k} = \frac{\sum_{\substack{i\in\{neutrals\}\\ j\in\{neutrals\}}} F_{ijk} + \beta}{\sum_{\substack{i\in\{neutrals\}\\ j\in\{neutrals\}}} F_{ijh} + \beta}$$

Finally, to infer each single mutant fitness (*W*), barcode relative abundance of each strain was contrasted with the relative abundance inferred for wild type:

$$W_{ik} = \frac{R_{ik}}{R_{wt,k}} \quad \text{and} \quad W_{jk} = \frac{R_{jk}}{R_{wt,k}}$$

Inference of double mutant abundance

Similar to the single mutant metrics, we used the double mutant relative abundance to calculate strain changes over time:

$$R_{ijk} = \frac{F_{ijk} + \beta}{F_{ijh} + \beta}$$

Furthermore, we compared the normalized double mutant values to wild type values to derive double mutant fitness:

$$W_{ijk} = \frac{R_{ijk}}{R_{wt,k}}$$

Genetic Interaction Score

Our genetic interaction score was inspired by the multiplicative model that is now commonly used to score genetic interactions [1]:

$$GIS = W_{ijk} - W_{ik} \times W_{jk}$$

GIS values smaller than zero represent negative genetic interactions, whereas those above zero represent positive genetic interactions. To contrast genetic interactions between condition pairs in Fig 3, we obtained a Z-score for GIS within each condition and used an absolute GIS = 1 as cutoff.

Acknowledgements

We are grateful for helpful comments from Yong Lu, Michael Principato, Ramamurthy Mani, and Meng Xiao He at the outset of this project. To Brenda Andrews and Charlie Boone labs for reagents donation and insightful comments during this study. And to the Roth lab members for support and feedback over the duration of this project.

Funding Disclosure

We gratefully acknowledge support by the Canadian Excellence Research Chairs (CERC) Program (to F.P.R.), by the Canadian Institutes of Health Research (MOP-79368 to G.W.B.), by the National Human Genome Research Institute of the National Institutes of Health (NIH/NHGRI) HG004756, and by an individual NRSA award (HG004825) to J.C.M.. F.P.R. was also supported by a NIH/NHGRI Center of Excellence in Genomic Science (HG004233), by NIH/NHGRI grant HG001715, and by the One Brave Idea Foundation.

Figure Legends

Fig 1. BFG-GI Pipeline Summary

(A) Construction of donors with unique barcodes representing each gene deletion in parental strains from the YKO collection. **(B)** Construction of recipients also with unique barcodes representing genes of interest in parental strains from the SGA query collection. Barcodes from both, donors and recipients were flanked by *loxP/lox2272* sites to allow in-vivo intracellular fusion of barcode pairs. **(C)** Donors and recipients were mated with each other to generate heterozygous diploid double mutants and barcodes were fused *in vivo* by the Cre/Lox system. The relic plasmid remaining in donors after Cre/Lox recombination was eliminated after barcode fusion. Sporulation was induced to select for the *MAT***a** progeny and haploid double mutants. **(D)** BFG-GI was conducted *en masse* to generate 'many-by-many' pools for a set of 26 DNA repair and 14 neutral genes. The resulting pool of haploid double mutants was stored as glycerol stock, from which aliquots were used to inoculate media containing different chemical agents ('drugs'). Genomic DNA was extracted and fused barcodes were amplified and sequenced to monitor double mutant abundance and to infer genetic interactions. Details of Donor and Recipient strain construction are shown in S1 Fig and S2 Fig, respectively. Media details are shown in S3 Fig.

Fig 2. BFG-GI Quality Control and Benchmarking

(A) Histograms and scatter plot analysis shows the correlation between two measures of cell abundance—colony size and next-generation-sequencing-based quantitation of fused barcodes—for a matrix of BFG-GI double mutant strains. Peaks in the histograms representing data points in the bottom-left corner of the scatter plot indicate that absent and very small colonies produced few or no sequencing reads. **(B)** Density plots for BFG-GI genetic interaction score (GIS) correlation between replicates of the same gene, with same or different parental origin, or pairs of different genes. Only replicates with a GIS correlation > 0.5 were retained for further analyses. **(C)** Comparison of BFG-GI-inferred genetic interactions in haploid double mutant media without MMS with genetic interactions identified using similar media [8]. **(D)** Comparison of BFG-GI-inferred genetic interactions in haploid double mutant media containing MMS with genetic interactions previously identified in similar media [8]. **(E)** Benchmarking of BFG-GI genetic interactions against the St. Onge *et al.* dataset [8]. **(F)** Density plot comparing the GIS distribution for same-gene pairs (which are expected to behave like synthetic lethals given the SGA double-mutant selection process) with that for linked and unlinked gene pairs.

Fig 3. Condition Dependent Genetic Interactions Mapped by BFG-GI

(A) Networks showing the number of conditions with a genetic interaction for each gene pair (using the criteria Z < -1 for negative GIS and Z > 1 for positive GIS). Numbers besides gene names are guides for the reader to locate nodes in networks of panels (B) and (C). **(B)** Networks in the diagonal (subpanels *ii* and *iii*) show

genetic interactions (GIs) for DMSO or MMS after applying the same Z-score criteria as in (A). The network in subpanel *i* shows how the genetic interactions change when DMSO and MMS treatments are compared. Interaction signs can be positive (+), negative (-), or neutral (n). The barplot in subpanel *iv* summarizes the number of sign changes in subpanel *iii*. **(C)** The networks are the same as described in (B) with additional drug conditions: cisplatin (CSPL), camptothecin (CMPT), doxorubicin (DXRB), hydroxyurea (HYDX), zeocin (ZEOC), bleomycin (BLMC) and 4NQO. The no-drug condition was omitted from this figure, as it was very similar to the DMSO treatment (S2 Table).

Fig 4. Shu Complex Condition-Dependent Genetic Interactions with *MAG1*, *SLX4*, *PPH3* and *RAD53*

(A) Pleiotropic participation of the Shu complex in DNA replication and repair pathways. **(B)** Network showing condition-dependent genetic interactions inferred from BFG-GI for the indicated conditions. **(C)** Confirmation of interactions between the Shu complex, *MAG1* and *SLX4* using spot dilution assays including single and double mutants exposed to the indicated drugs. Orange, blue, and red boxes indicate genetic interactions of Shu complex members with *MAG1* and *SLX4*, and of *MAG1* with *SLX4*, respectively. **(D)** Schematic of potential functional connections between the Shu complex and *SLX4.* As with deletion of *SLX4* or *PPH3*, deletion of Shu complex members may lead to hyperphosphorylation and hyperactivation of Rad53, resulting in increased sensitivity to MMS. **(E)** Spot dilution assays showing genetic interactions of Shu/*pph3Δ* double mutants exposed to MMS. Shu complex single

mutants are shown in panel (C). **(F)** Western blot assays showing hyperphosphorylation of Rad53 in *csm2Δ, psy3Δ, shu1Δ,* and *slx4Δ* strains following treatment with 0.03% MMS. Note increased intensity of Rad53-P bands compared with the Rad53 bands. **(G)** Spot dilution assays showing decreased MMS sensitivity of Shu complex mutants expressing a hypomorphic *rad53-R605A* allele (*rad53-R605A-6xHis-3xFLAG-kanMX6*) compared with a wild type *RAD53* allele (*RAD53-6xHis-3xFLAG-kanMX6)*.

Supporting Information

S1 Fig. Donor Toolkit Construction

Two fragments were built to generate proDonor plasmids. The first, preD1, contained *loxP/lox2272* sites flanking unique barcodes and a hygromycin resistance marker **(A)**. The second, preD2, contained the Cre recombinase driven by the doxycycline inducible *tetO-CMV*, and a *URA3* marker **(B)**. The two fragments were assembled *in vivo* by yeast to generate pDonors **(C)**, which were arrayed and Sanger sequenced to confirm the integrity of the preD1 fragment **(D)**. ProDonors with confirmed preD1 fragments were mated with YKO strains to generate strains carrying both a uniquely barcoded pDonor and a gene deletion of interest. Then they were sporulated and the haploid *MAT*alpha progeny was selected using the mating type maker indicated in (C). Details on selective media are shown in S3 Fig.

S2 Fig. Recipient Toolkit Construction

Two constructs were built to generate recipients. The first fragment, preR1, contained *loxP/lox2272* sites flanking unique barcodes and a *klURA3* marker **(A)**. The second construct, preR2, contained the *can1Δ::*P_{STE2}*-spHis5-*T_{STE2} mating type marker **(B)**. The two fragments were assembled *in vivo* using a derivative of the *delitto perfetto* construct **(C)**. Resulting proRecipients were arrayed and Sanger sequenced to confirm integrity of preR1 loci **(D)**. ProRecipients with confirmed preR1 loci were mated with SGA query strains to generate strains carrying both a uniquely barcoded recipient construct and a gene-deletion of interest. Then they

were sporulated and the haploid *MAT***a** progeny was selected using the mating type maker indicated in (C). Details on selective media are shown in S3 Fig.

S3 Fig. Media Details to Generate BFG-GI Strains and Pools

Donors, recipients and double mutants used in BFG-GI were generated as shown in Fig 1, S1 Fig and S2 Fig. This figure shows media details, optimal inoculum cell densities, and incubation times for pool-based cultures. All incubations were at 30°C for 24 hrs, except for mating (12 hrs at 23°C) and sporulation (12 days at 21°C). Sporulation was conducted in flasks with liquid media shaking at 200rpm. We used the following reagent concentrations: G418=200 µg/mL, clonNat=100 µg/mL, canavanine=100 µg/mL, thialysine=100 µg/mL, hygromycin=200 µg/mL, 5-FOA=1 mg/mL. Amino acid concentrations were as described in [10].

S4 Fig. Strains and Genes in BFG-GI Pools

Sixty Donors, representing 34 genes and 56 Recipients, representing 38 genes were crossed all-vs-all as a pool. The first number in the parentheses is the total number of strains and the second number in the parentheses is the number of genes. Single mutant fitness was inferred from double mutant fitness measurements corresponding to one DNA repair- and one neutral gene. Similarly, the neutral-neutral double mutants were used to infer the wild type fitness.

S1 Table. BFI-GI Tested Conditions

Description of conditions tested, including drug names, concentrations and vendor codes.

S2 Table. BFI-GI Raw Sequencing Measurements and GIS

Raw numbers of next-generation sequencing reads measured for each double mutant across all conditions and derived GISs

References

1. Mani R, St Onge RP, Hartman JL, Giaever G, Roth FP. Defining genetic interaction. Proc Natl Acad Sci U S A. 2008;105: 3461–3466. doi:10.1073/pnas.0712255105

2. Baryshnikova A, Costanzo M, Kim Y, Ding H, Koh J, Toufighi K, et al. Quantitative analysis of fitness and genetic interactions in yeast on a genome scale. Nat Methods. 2010;7: 1017–1024. doi:10.1038/nmeth.1534

3. Ideker T, Krogan NJ. Differential network biology. Mol Syst Biol. 2012;8: 565. doi:10.1038/msb.2011.99

4. Bandyopadhyay S, Mehta M, Kuo D, Sung M-K, Chuang R, Jaehnig EJ, et al. Rewiring of genetic networks in response to DNA damage. Science. 2010;330: 1385–1389. doi:10.1126/science.1195618

5. Costanzo M, Baryshnikova A, Bellay J, Kim Y, Spear ED, Sevier CS, et al. The genetic landscape of a cell. Science. 2010;327: 425–431. doi:10.1126/science.1180823

6. Costanzo M, VanderSluis B, Koch EN, Baryshnikova A, Pons C, Tan G, et al. A global genetic interaction network maps a wiring diagram of cellular function. Science. 2016;353. doi:10.1126/science.aaf1420

7. van Leeuwen J, Pons C, Mellor JC, Yamaguchi TN, Friesen H, Koschwanez J, et al. Exploring genetic suppression interactions on a global scale. Science. 2016;354. doi:10.1126/science.aag0839

8. St Onge RP, Mani R, Oh J, Proctor M, Fung E, Davis RW, et al. Systematic pathway analysis using high-resolution fitness profiling of combinatorial gene deletions. Nat Genet. 2007;39: 199–206. doi:10.1038/ng1948

9. Giaever G, Chu AM, Ni L, Connelly C, Riles L, Véronneau S, et al. Functional profiling of the Saccharomyces cerevisiae genome. Nature. 2002;418: 387–391. doi:10.1038/nature00935

10. Tong AH, Boone C. Synthetic Genetic Array SGA Analysis in Saccharomyces cerevisiae. Yeast Protocols. 2nd ed. Totowa, NJ: The Humana Press Inc.; 2005. pp. 171–192.

11. Collins SR, Schuldiner M, Krogan NJ, Weissman JS. A strategy for extracting and analyzing large-scale quantitative epistatic interaction data. Genome Biol. 2006;7: R63. doi:10.1186/gb-2006-7-7-r63

12. DeLuna A, Vetsigian K, Shoresh N, Hegreness M, Colón-González M, Chao S, et al. Exposing the fitness contribution of duplicated genes. Nat Genet. 2008;40: 676–681. doi:10.1038/ng.123

13. Garay E, Campos SE, González de la Cruz J, Gaspar AP, Jinich A, Deluna A. High-resolution profiling of stationary-phase survival reveals yeast longevity factors and their genetic interactions. PLoS Genet. 2014;10: e1004168. doi:10.1371/journal.pgen.1004168

14. Jaffe M, Sherlock G, Levy SF. iSeq: A New Double-Barcode Method for Detecting Dynamic Genetic Interactions in Yeast. G3 Bethesda Md. 2017;7: 143–153. doi:10.1534/g3.116.034207

15. Pan X, Yuan DS, Xiang D, Wang X, Sookhai-Mahadeo S, Bader JS, et al. A robust toolkit for functional profiling of the yeast genome. Mol Cell. 2004;16: 487–496. doi:10.1016/j.molcel.2004.09.035

16. Decourty L, Saveanu C, Zemam K, Hantraye F, Frachon E, Rousselle J-C, et al. Linking functionally related genes by sensitive and quantitative characterization of genetic interaction profiles. Proc Natl Acad Sci U S A. 2008;105: 5821–5826. doi:10.1073/pnas.0710533105

17. Claussen CA, Long EC. Nucleic Acid recognition by metal complexes of bleomycin. Chem Rev. 1999;99: 2797–2816.

18. Ball LG, Zhang K, Cobb JA, Boone C, Xiao W. The yeast Shu complex couples error-free post-replication repair to homologous recombination. Mol Microbiol. 2009;73: 89–102. doi:10.1111/j.1365-2958.2009.06748.x

19. Bernstein KA, Reid RJD, Sunjevaric I, Demuth K, Burgess RC, Rothstein R. The Shu complex, which contains Rad51 paralogues, promotes DNA repair through inhibition of the Srs2 anti-recombinase. Mol Biol Cell. 2011;22: 1599–1607. doi:10.1091/mbc.E10-08-0691

20. Godin S, Wier A, Kabbinavar F, Bratton-Palmer DS, Ghodke H, Van Houten B, et al. The Shu complex interacts with Rad51 through the Rad51 paralogues Rad55-Rad57 to mediate error-free recombination. Nucleic Acids Res. 2013;41: 4525–4534. doi:10.1093/nar/gkt138

21. Mankouri HW, Ngo H-P, Hickson ID. Shu proteins promote the formation of homologous recombination intermediates that are processed by Sgs1-Rmi1-Top3. Mol Biol Cell. 2007;18: 4062–4073. doi:10.1091/mbc.E07-05-0490

22. Sasanuma H, Tawaramoto MS, Lao JP, Hosaka H, Sanda E, Suzuki M, et al. A new protein complex promoting the assembly of Rad51 filaments. Nat Commun. 2013;4: 1676. doi:10.1038/ncomms2678

23. Berdal KG, Bjørås M, Bjelland S, Seeberg E. Cloning and expression in Escherichia coli of a gene for an alkylbase DNA glycosylase from Saccharomyces cerevisiae; a homologue to the bacterial alkA gene. EMBO J. 1990;9: 4563–4568.

24. Chen J, Derfler B, Samson L. Saccharomyces cerevisiae 3-methyladenine DNA glycosylase has homology to the AlkA glycosylase of E. coli and is induced in response to DNA alkylation damage. EMBO J. 1990;9: 4569–4575.

25. Flott S, Alabert C, Toh GW, Toth R, Sugawara N, Campbell DG, et al. Phosphorylation of Slx4 by Mec1 and Tel1 regulates the single-strand annealing mode of DNA repair in budding yeast. Mol Cell Biol. 2007;27: 6433–6445. doi:10.1128/MCB.00135-07

26. Fricke WM, Brill SJ. Slx1-Slx4 is a second structure-specific endonuclease functionally redundant with Sgs1-Top3. Genes Dev. 2003;17: 1768–1778. doi:10.1101/gad.1105203

27. Gritenaite D, Princz LN, Szakal B, Bantele SCS, Wendeler L, Schilbach S, et al. A cell cycle-regulated Slx4-Dpb11 complex promotes the resolution of DNA repair intermediates linked to stalled replication. Genes Dev. 2014;28: 1604–1619. doi:10.1101/gad.240515.114

28. Toh GW-L, Sugawara N, Dong J, Toth R, Lee SE, Haber JE, et al. Mec1/Tel1-dependent phosphorylation of Slx4 stimulates Rad1-Rad10-dependent cleavage of non-homologous DNA tails. DNA Repair. 2010;9: 718–726. doi:10.1016/j.dnarep.2010.02.013

29. Jablonowski CM, Cussiol JR, Oberly S, Yimit A, Balint A, Kim T, et al. Termination of Replication Stress Signaling via Concerted Action of the Slx4 Scaffold and the PP4 Phosphatase. Genetics. 2015;201: 937–949. doi:10.1534/genetics.115.181479

30. Ohouo PY, Bastos de Oliveira FM, Liu Y, Ma CJ, Smolka MB. DNA-repair scaffolds dampen checkpoint signalling by counteracting the adaptor Rad9. Nature. 2013;493: 120–124. doi:10.1038/nature11658

31. Godin SK, Zhang Z, Herken BW, Westmoreland JW, Lee AG, Mihalevic MJ, et al. The Shu complex promotes error-free tolerance of alkylation-induced base excision repair products. Nucleic Acids Res. 2016;44: 8199–8215. doi:10.1093/nar/gkw535

32. Huang D, Piening BD, Paulovich AG. The preference for error-free or error-prone postreplication repair in Saccharomyces cerevisiae exposed to low-dose methyl methanesulfonate is cell cycle dependent. Mol Cell Biol. 2013;33: 1515–1527. doi:10.1128/MCB.01392-12

33. Xu X, Ball L, Chen W, Tian X, Lambrecht A, Hanna M, et al. The yeast Shu complex utilizes homologous recombination machinery for error-free lesion bypass via physical interaction with a Rad51 paralogue. PloS One. 2013;8: e81371. doi:10.1371/journal.pone.0081371

34. Cussiol JR, Jablonowski CM, Yimit A, Brown GW, Smolka MB. Dampening DNA damage checkpoint signalling via coordinated BRCT domain interactions. EMBO J. 2015;34: 1704–1717. doi:10.15252/embj.201490834

35. Pfander B, Diffley JFX. Dpb11 coordinates Mec1 kinase activation with cell cycle-regulated Rad9 recruitment. EMBO J. 2011;30: 4897–4907. doi:10.1038/emboj.2011.345

36. O'Neill BM, Szyjka SJ, Lis ET, Bailey AO, Yates JR, Aparicio OM, et al. Pph3-Psy2 is a phosphatase complex required for Rad53 dephosphorylation and replication fork restart during recovery from DNA damage. Proc Natl Acad Sci U S A. 2007;104: 9290–9295. doi:10.1073/pnas.0703252104

37. Balint A, Kim T, Gallo D, Cussiol JR, Bastos de Oliveira FM, Yimit A, et al. Assembly of Slx4 signaling complexes behind DNA replication forks. EMBO J. 2015;34: 2182–2197. doi:10.15252/embj.201591190

38. Soellick TR, Uhrig JF. Development of an optimized interaction-mating protocol for large-scale yeast two-hybrid analyses. Genome Biol. 2001;2: RESEARCH0052.

39. Codon AC, Gasent-Ramirez JM, Benitez T. Factors Which Affect the Frequency of Sporulation and Tetrad Formation in Saccharomyces cerevisiae Baker's Yeasts. Appl Environ Microbiol. 1995;61: 1677.

40. Tong AH, Boone C. High-Throughput Strain Construction and Systematic Synthetic Lethal Screening in Saccharomyces cerevisiae. Methods Microbiol. 2007;36: 369–707.

41. Gibson DG. Synthesis of DNA fragments in yeast by one-step assembly of overlapping oligonucleotides. Nucleic Acids Res. 2009;37: 6984–6990. doi:10.1093/nar/gkp687

42. Storici F, Resnick MA. The delitto perfetto approach to in vivo site-directed mutagenesis and chromosome rearrangements with synthetic oligonucleotides in yeast. Methods Enzymol. 2006;409: 329–345. doi:10.1016/S0076-6879(05)09019-1

43. Ha G, Roth A, Lai D, Bashashati A, Ding J, Goya R, et al. Integrative analysis of genome-wide loss of heterozygosity and monoallelic expression at nucleotide resolution reveals disrupted pathways in triple-negative breast cancer. Genome Res. 2012;22: 1995–2007. doi:10.1101/gr.137570.112

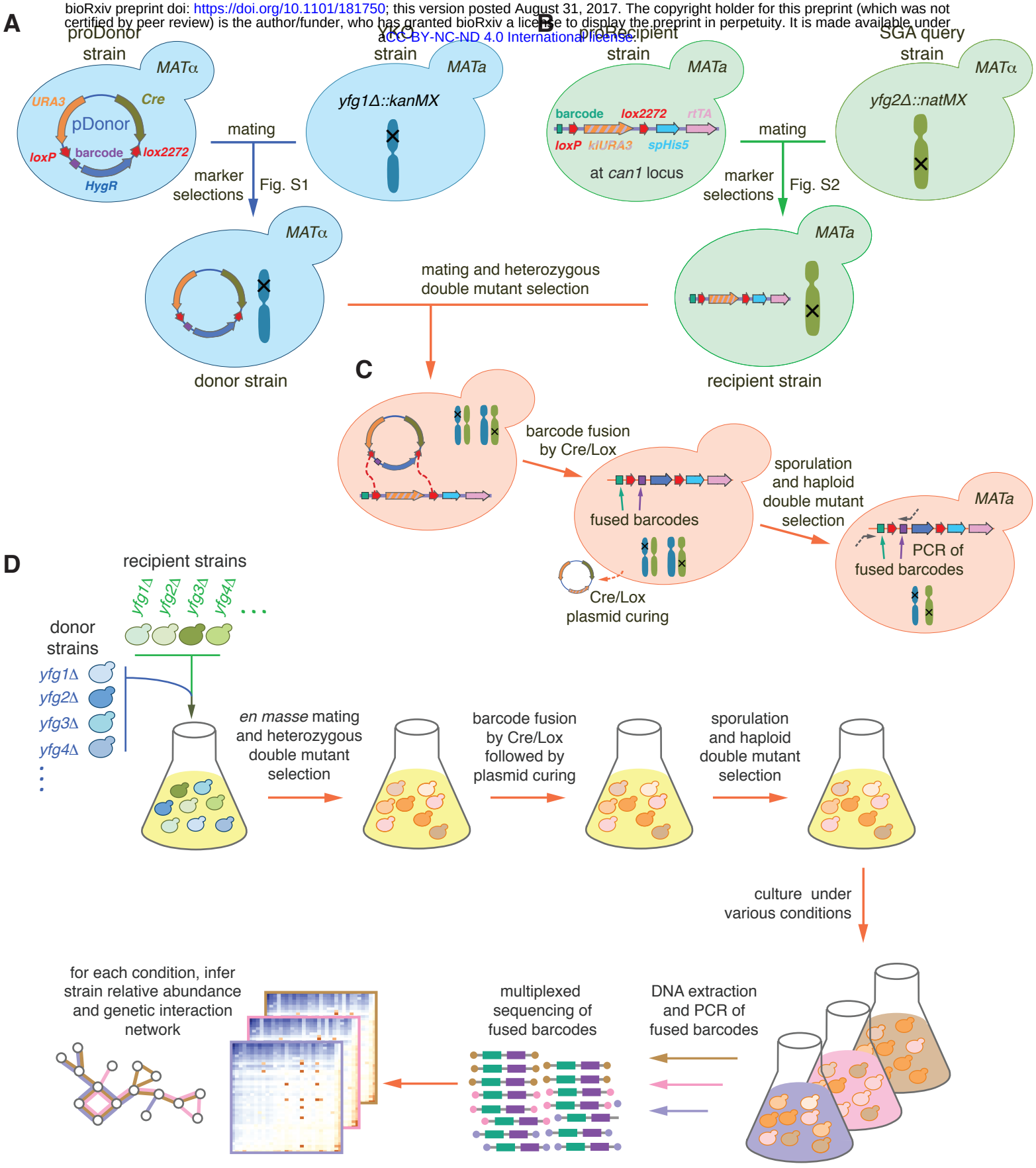

Figure 1

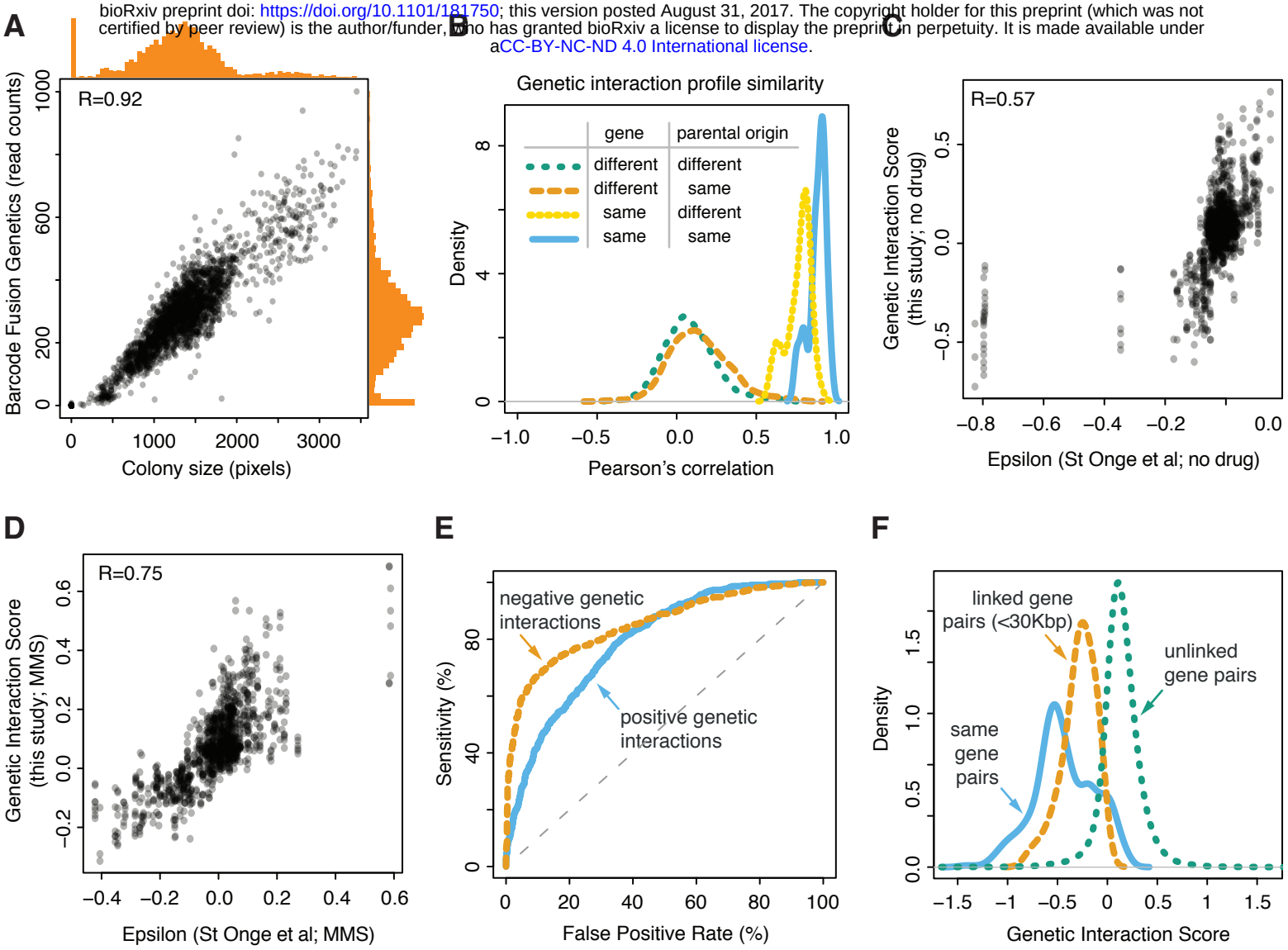

Figure 2

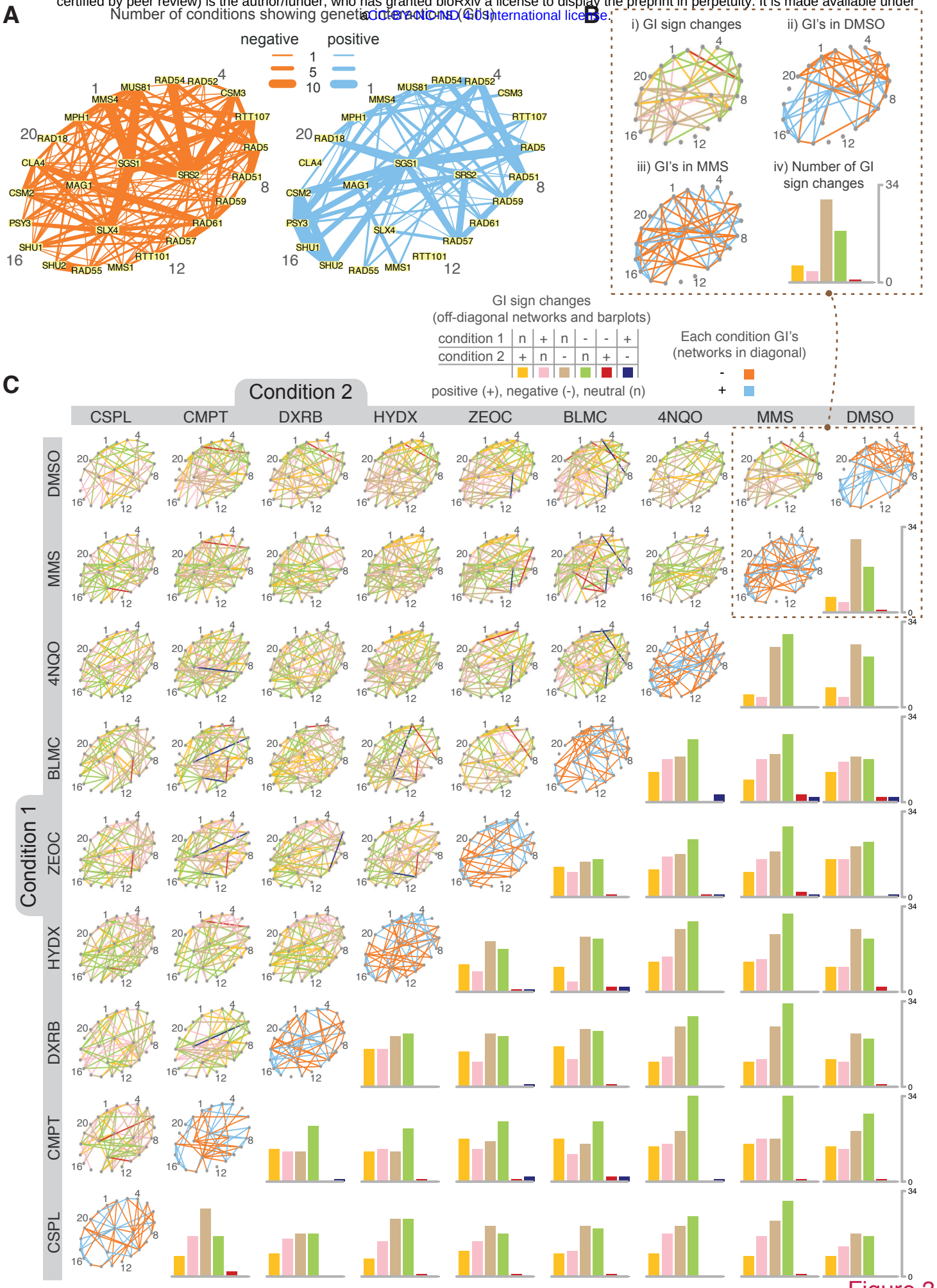

Figure 3

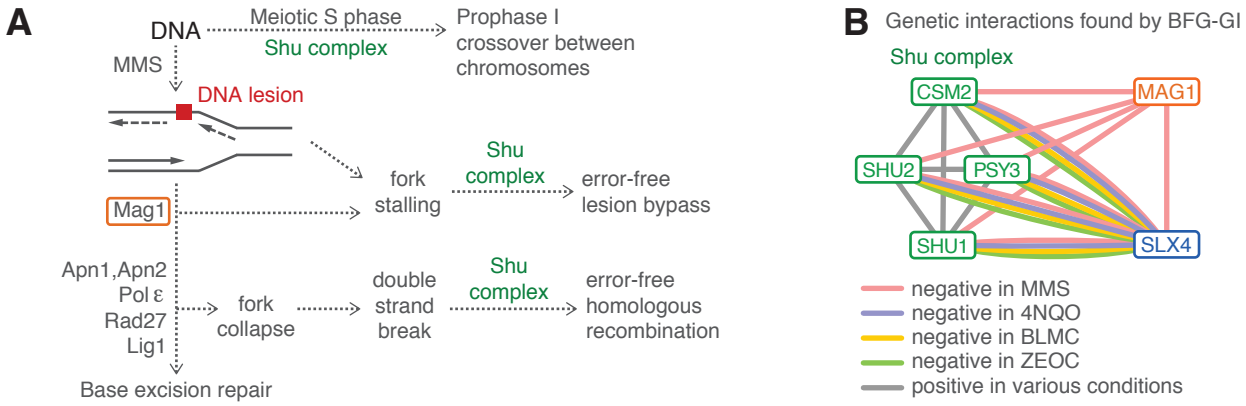

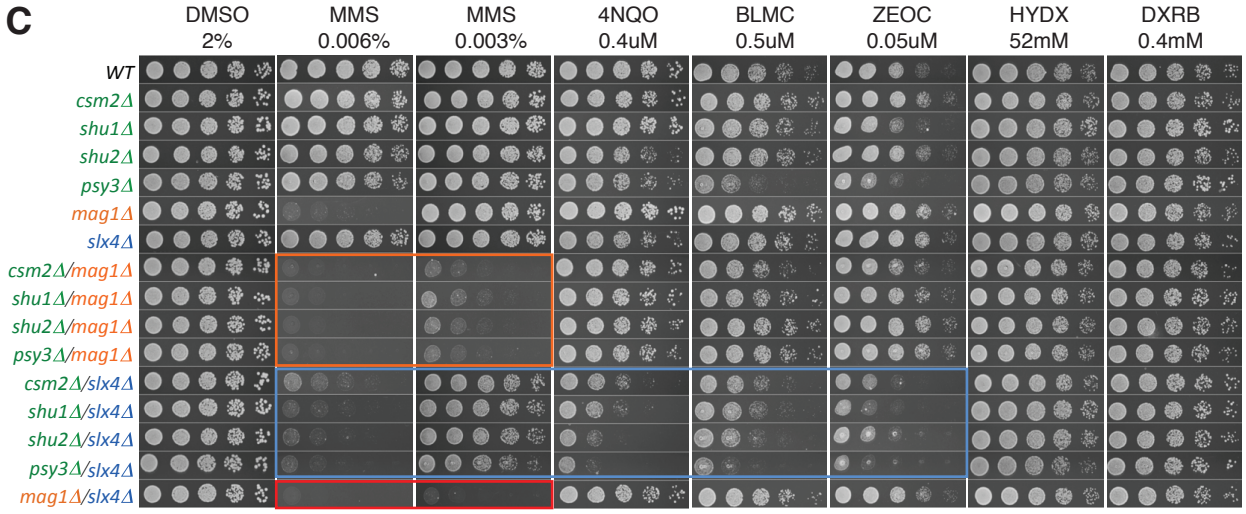

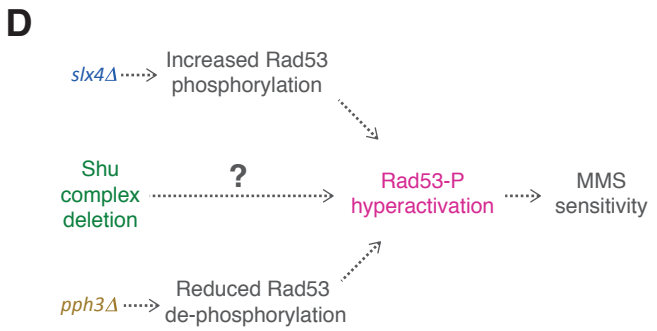

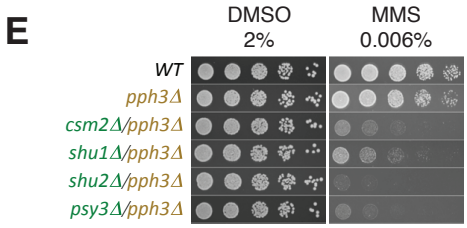

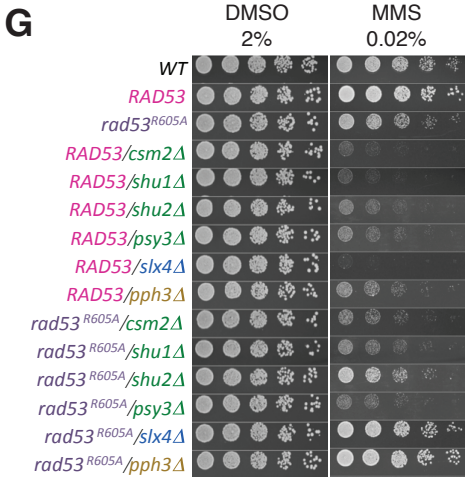

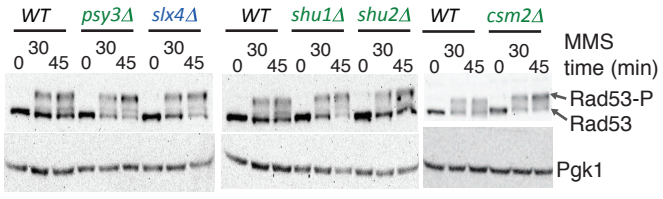

Figure 4

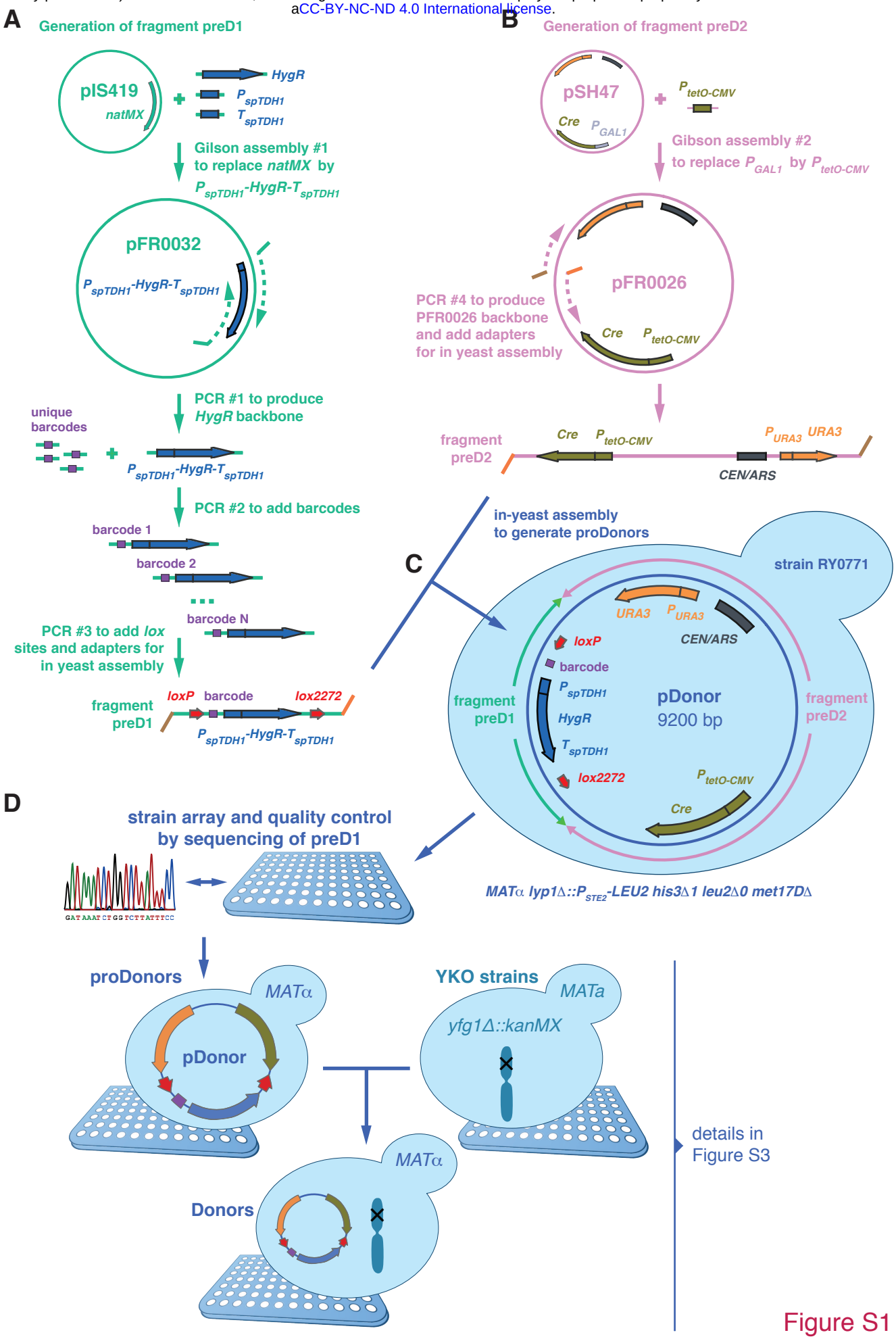

Figure S1

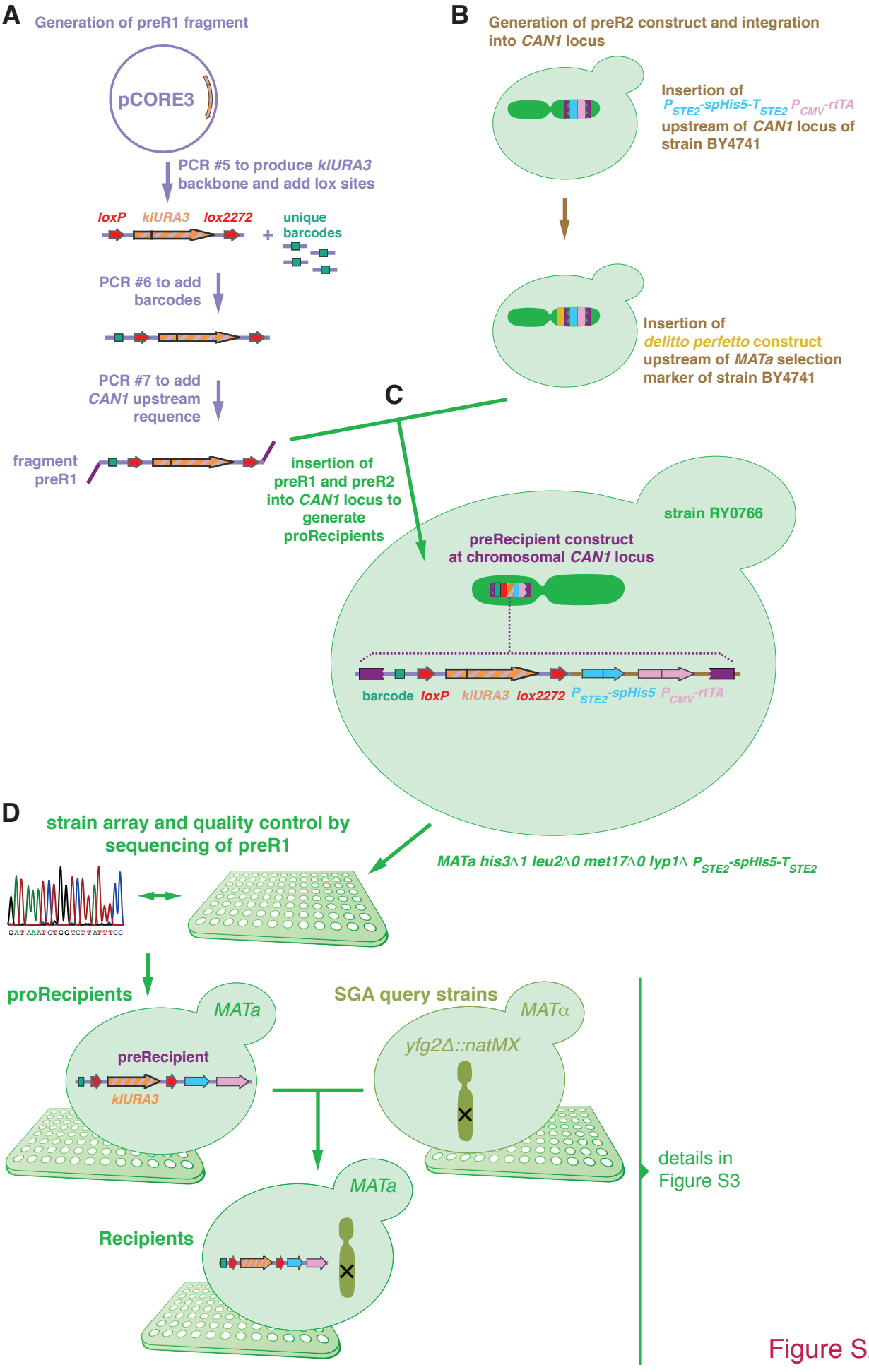

Figure S2

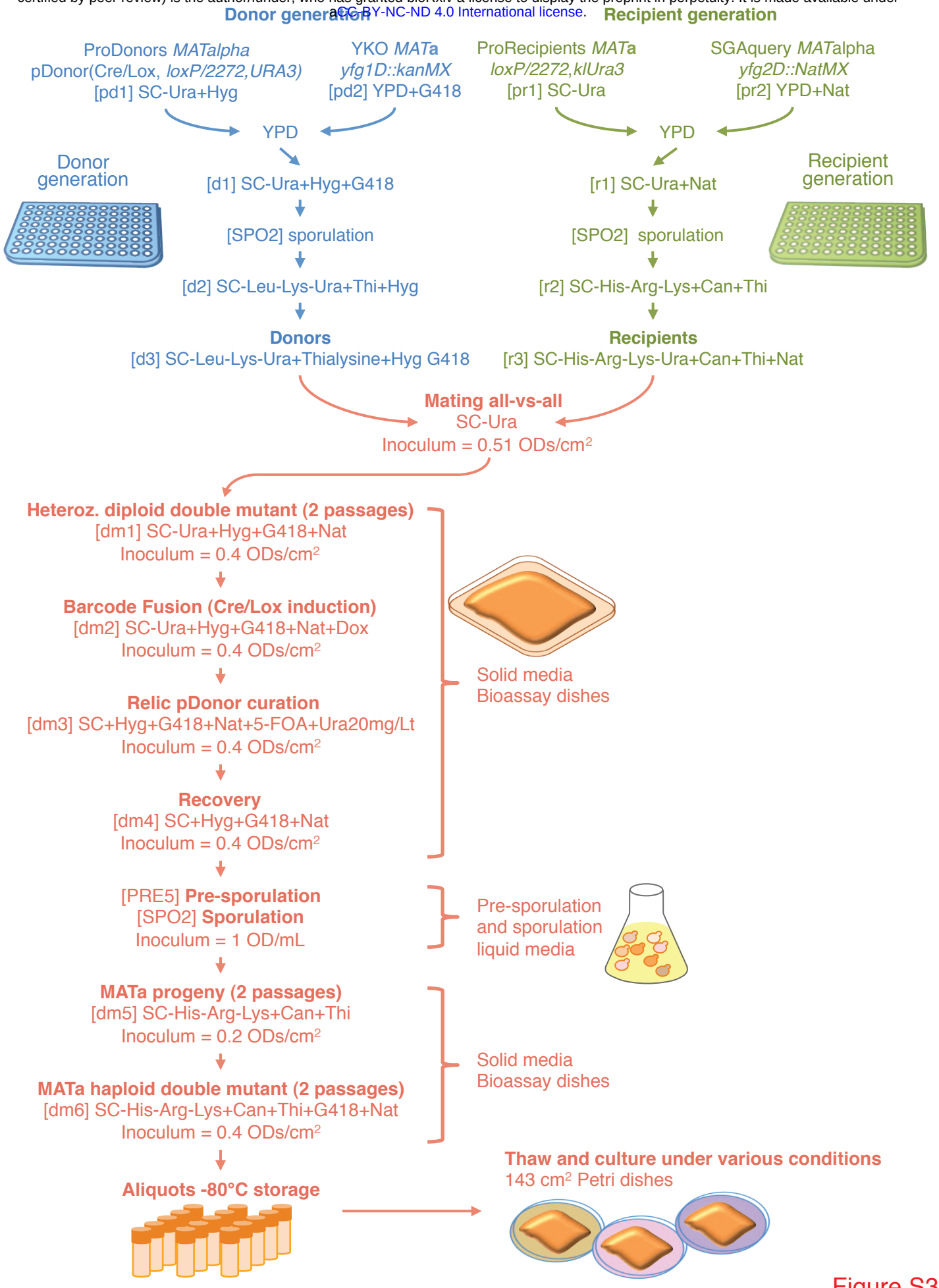

Figure S3

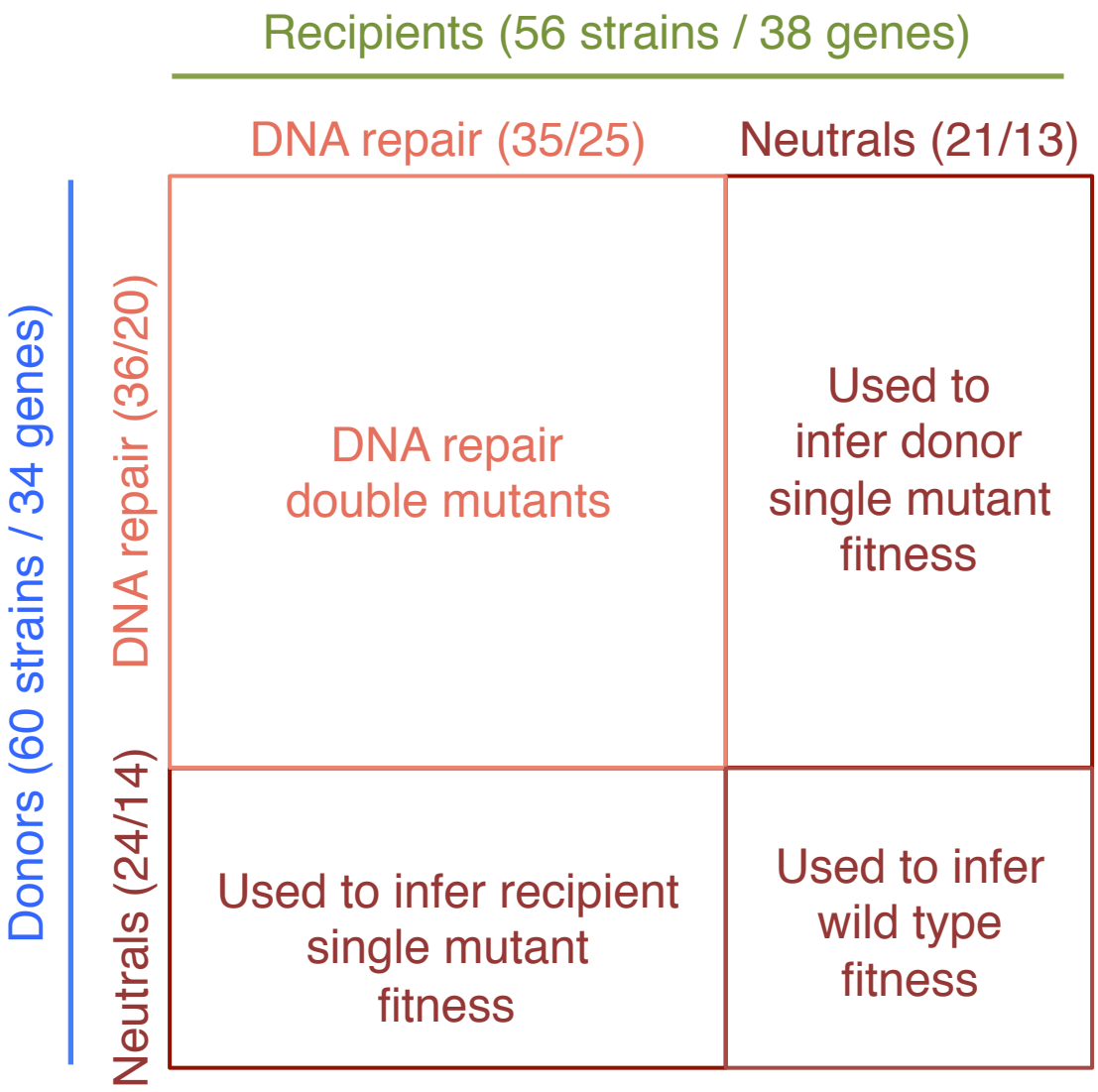

Figure S4